

Formation of coffee-stain patterns at the nanoscale: The role of nanoparticle solubility and solvent evaporation rate

Cite as: J. Chem. Phys. **146**, 114503 (2017); <https://doi.org/10.1063/1.4978284>

Submitted: 16 November 2016 . Accepted: 24 February 2017 . Published Online: 21 March 2017

Jianguo Zhang, Jasmin Milzetti,  Frédéric Leroy, and Florian Müller-Plathe



View Online



Export Citation



CrossMark

ARTICLES YOU MAY BE INTERESTED IN

[Evaporation induced self-assembly of different shapes and sizes of nanoparticles: A molecular dynamics study](#)

The Journal of Chemical Physics **150**, 044708 (2019); <https://doi.org/10.1063/1.5053974>

[Molecular dynamics simulations of evaporation-induced nanoparticle assembly](#)

The Journal of Chemical Physics **138**, 064701 (2013); <https://doi.org/10.1063/1.4789807>

[Droplet evaporation with complexity of evaporation modes](#)

Applied Physics Letters **110**, 031602 (2017); <https://doi.org/10.1063/1.4974292>

Challenge us.

What are your needs for periodic signal detection?



Zurich
Instruments

Formation of coffee-stain patterns at the nanoscale: The role of nanoparticle solubility and solvent evaporation rate

Jianguo Zhang,^{a,b)} Jasmin Milzetti, Frédéric Leroy, and Florian Müller-Plathe

Eduard-Zintl-Institut für Anorganische und Physikalische Chemie and Profile Area Thermo-Fluids & Interfaces, Technische Universität Darmstadt, Alarich-Weiss-Straße 8, D-64287 Darmstadt, Germany

(Received 16 November 2016; accepted 24 February 2017; published online 21 March 2017)

When droplets of nanoparticle suspension evaporate from surfaces, they leave behind a deposit of nanoparticles. The mechanism of evaporation-induced pattern formation in the deposit is studied by molecular dynamics simulations for sessile nanodroplets. The influence of the interaction between nanoparticles and liquid molecules and the influence of the evaporation rate on the final deposition pattern are addressed. When the nanoparticle-liquid interaction is weaker than the liquid-liquid interaction, an interaction-driven or evaporation-induced layer of nanoparticles appears at the liquid-vapor interface and eventually collapses onto the solid surface to form a uniform deposit independently of the evaporation rate. When the nanoparticle-liquid and liquid-liquid interactions are comparable, the nanoparticles are dispersed inside the droplet and evaporation takes place with the contact line pinned at a surface defect. In such a case, a pattern with an approximate ring-like shape is found with fast evaporation, while a more uniform distribution is observed with slower evaporation. When the liquid-nanoparticle interaction is stronger than the liquid-liquid interaction, evaporation always occurs with receding contact line. The final deposition pattern changes from volcano-like to pancake-like with decreasing evaporation rate. These findings might help to design nanoscale structures like nanopatterns or nanowires on surface through controlled solvent evaporation. Published by AIP Publishing. [http://dx.doi.org/10.1063/1.4978284]

I. INTRODUCTION

The coffee-ring effect refers to a ring-like deposition pattern of drying droplets of complex fluids.¹ For practical applications, this inhomogeneous ring-like structure is sometimes desired like in the fabrication of nanowires² and sometimes undesired in processes like coating³ and ink-jet printing.⁴ It is therefore of great significance to understand the basic mechanism of pattern formation of drying droplets if one wants to control the deposition pattern. Deegan *et al.*^{1,5} proposed that two main causes are responsible for the coffee-ring effect (i) the pinned contact line of the evaporating droplet and (ii) the non-uniform evaporation rate along the droplet interface. Taken together, these two factors introduce an outwards capillary flow which drives particles towards the droplet edge, leading to a ring-like structure of the deposited particles. Hu and Larson⁶ later pointed out that Marangoni flow along the liquid-vapor interface was also important and it can suppress the coffee-ring pattern by bringing the particles back from the three-phase contact line (TPCL) area to the bulk. The interplay between the outward capillary flow and the inward Marangoni flow leads to a recirculation loop inside the droplet. Such a loop could produce a uniform pattern after the complete evaporation of the droplet. The Marangoni flow can basically be generated by a gradient of interfacial tension, which results from a

temperature gradient^{7,8} and/or a surfactant-concentration gradient⁹ along the liquid-vapor interface. Alternatively, electrowetting has been successfully used to control the shape of the deposition pattern^{10,11} by applying relatively high frequency currents. Moving contact lines and strong internal flows were found to counterbalance the coffee-ring effect, and uniform deposition patterns were eventually observed.

As a matter of fact, the evaporation of a droplet with solutes is a very complex phenomenon and the deposit patterns are very diverse.^{12,13} In very recent years, intensive research has been carried out, and the influence of many other factors than those mentioned above on the deposition patterns has been explored. For instance, it has been reported¹⁴ that smaller particles formed a uniform distribution while larger ones formed a coffee-ring structure. Particle-sorting phenomena based on their sizes were also observed.¹⁵ The important role of the particle shape played¹⁶ on the deposition pattern was also discussed. It was found that spherical particles formed a ring-like structure while ellipsoidal particles could form a uniform stain. Besides, high concentrations¹⁷ of particles formed a coffee-ring, while low concentrations formed a petal-like structure. Furthermore, the pattern changed from a ring-like to a uniform distribution by applying an acoustic field.¹⁸ Very recently, the evaporation rate¹⁹ has been experimentally found to play an important role in the final pattern. In contrast to slow evaporation which led to the formation of a coffee ring, fast evaporation yielded uniform deposits whose origin is the evaporation-induced formation of a layer of nanoparticles at the liquid-vapor interface. Note that the experimental studies all apply to macroscopic ($>100 \mu\text{m}$ in diameter) droplets of

^{a)}Author to whom correspondence should be addressed. Electronic mail: j.zhang@theo.chemie.tu-darmstadt.de

^{b)}Present address: Max-Planck-Institut für Polymerforschung, Ackermannweg 10, D-55122 Mainz, Germany.

nano particle suspensions, with droplets of nano-dimensions being difficult to access experimentally.

The nanosize regime has been covered by several theoretical and simulations studies,^{20–27} aimed at understanding the basic mechanisms of particle deposition through evaporation. For example, by increasing the motion of the contact line and decreasing the evaporation rate in a numerical calculation, Man and Doi²⁰ reported a continuous change of the shape of the deposit pattern from a ring-like to volcano-like and further to mountain-like. Crivoi *et al.*^{26,27} developed a Monte-Carlo-like model and found that increasing the particle-particle interaction and particle adsorption at the gas-liquid interface could suppress the coffee-ring effect. By molecular dynamics simulations, Chen *et al.*²³ showed that adding charges to the nanoparticle surface leads to the assembly of nanoparticles at the rim; Zhang *et al.*^{24,25} reported that higher solid-liquid interaction, slower evaporation rate, and higher salt ions concentration generate a ring-like deposit, and that such a ring structure can be changed by applying an electric field in salty-water nanodroplets.

This research's progress has definitely advanced our knowledge of the physical nature of pattern formation. However, the fundamental mechanisms behind are still far from being fully understood. For example, the solubility of the nanoparticles, which is controlled by the interaction of the particle with the solvent, has seldom been discussed in the literature. In the present study, we focus on the effect of the nanoparticle-liquid interaction and on the evaporation rate on the final deposit structures. This interaction was adjusted in a systematic way such that the solubility of the nanoparticles changed from insoluble to highly soluble. The model systems thus created serve to explore the effects of these parameters on the evaporation, rather than try to represent any specific real system. We comment how the evaporation behavior and the final deposition pattern depend on these parameters.

II. SIMULATION DETAILS

Figure 1(a) illustrates the simulation setup. A cylindrical droplet (periodic in the direction of view) containing nanoparticles was placed on a patterned solid substrate, which consists of two kinds of stripes (A and B) with different wetting properties.

The liquid, solid, and nanoparticles all consist of Lennard-Jones atoms for simplicity. The liquid is monatomic and one nanoparticle consists of 13 atoms (radius ≈ 1 nm) as shown in Fig. 1(b). The total non-bonded interaction energy was calculated with the 12-6 Lennard-Jones potential,

$$U_{pot} = \sum_{i=1}^N \sum_{j>i}^N 4\epsilon_{ij} \left[\left(\frac{\sigma_{ij}}{r_{ij}} \right)^{12} - \left(\frac{\sigma_{ij}}{r_{ij}} \right)^6 \right]. \quad (1)$$

In Eq. (1), N is the total number of particles. The i -th and j -th particles in the summation can be atoms of the liquid or the solid or they can belong to a nanoparticle. The interaction parameters σ_{ij} and ϵ_{ij} are the reduced parameters in Table I that refer to the corresponding interacting pairs. For example, if the i -th atom is a liquid atom and if the j -th atom belongs to a nanoparticle, σ_{ij} and ϵ_{ij} are the reduced parameters for the liquid-nanoparticle interaction with the values 0.8 and 1.1,

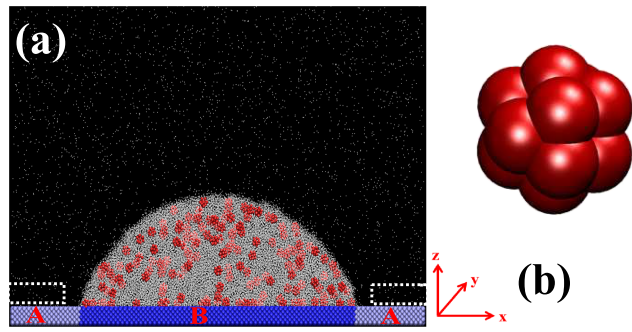


FIG. 1. (a) Cylindrical droplet of a suspension of nanoparticles (red) in a solvent (grey) on a solid substrate made of unwettable (A) and wettable (B) stripes. Gas-phase molecules are not shown. Dashed white rectangles mark the deletion zone. (b) Nanoparticle made up of 13 Lennard-Jones atoms. The VMD software²⁸ was used to produce these figures and all the subsequent snapshots.

respectively, indicated in line eight of Table I. The double sum in Eq. (1) does not include pair interactions within the nanoparticles. Rather, the nanoparticles were treated as rigid bodies throughout the simulations. The interaction parameters $\sigma = 0.3405$ nm and $\epsilon = 0.992$ kJ/mol for argon were used for the liquid-liquid interactions. The mass of the liquid atoms was $m = 6.63 \times 10^{-26}$ kg. In the following, all quantities are given in reduced units with respect to these parameters. The time unit is $\tau = \sqrt{m\sigma^2/\epsilon}$ and the reduced temperature $T^* = k_B T/\epsilon = 1$ corresponds to 119.8 K. The atoms of the substrate and the nanoparticles are ten times heavier than the liquid atoms. The reduced Lennard-Jones parameters for the solid-solid and liquid-solid interactions are listed in Table I.

Note that a much stronger interaction energy parameter for the solid-solid interactions than for the solid-liquid interactions was used to ensure that the substrate was kept stiff and smooth. The surface atoms of type B had a stronger interaction with liquid than the atoms of type A, making surface B more wettable than surface A. The equilibrium contact angles of droplets of the pure liquid at $T^* = 0.83$ on the pure surfaces A and B were $115.0^\circ \pm 6.9^\circ$ and $18.0^\circ \pm 2.2^\circ$, respectively.

TABLE I. Nonbonded interaction parameters for different interaction pairs in the simulated systems. All parameters are given in Lennard-Jones reduced units with respect to the parameters for the liquid-liquid interaction.

	ϵ^*	σ^*	Systems
Liquid-liquid	1.0	1.0	All
Solid-solid	10.0	1.2	All
Liquid-surface A	0.4	1.1	All
Liquid-surface B	0.9	1.1	All
Nanoparticle-surface A	0.4	1.1	All
Nanoparticle-surface B	0.9	1.1	All
Nanoparticle-nanoparticle	0.6	1.2	S1
Liquid-nanoparticle	0.8	1.1	S1
Nanoparticle-nanoparticle	0.8	1.2	S2
Liquid-nanoparticle	0.9	1.1	S2
Liquid-nanoparticle	1.0	1.1	S3
Nanoparticle-nanoparticle	1.0	1.2	S3
Liquid-nanoparticle	0.8	1.1	S4
Nanoparticle-nanoparticle	1.6	1.2	S4

Such a wetting contrast was set on purpose to pin the contact lines at the A-B boundary during evaporation to mimic the experimental pinning phenomenon of droplets' evaporation on heterogeneous surface, as proved in our previous simulations.²⁹ The effect of the interaction between the nanoparticles and liquid is the main focus in the present study. The corresponding interaction parameter ϵ was systematically adjusted such that the solubility of the nanoparticles changed from insoluble to highly soluble. In real experiments, this can be achieved by changing the type of nanoparticles or by the modification of their surface through coating. The four values 0.8, 0.9, 1.0, and 1.6 were chosen to induce that change in solubility in four different simulation systems as shown in Table I. The corresponding systems are denoted as S1, S2, S3, and S4, respectively. Note that the interaction between the nanoparticles was adjusted such that it was always smaller than the interaction between the nanoparticle and the liquid. If it were not the case, the nanoparticles would aggregate and form clusters.

The solid substrate is consisted of 10 800 atoms, one-third of which belonged to the unwettable strip A and the rest to strip B. All these atoms were packed into an FCC lattice with six layers. The box size was 171.5σ , 18.9σ , and 352.4σ in the x, y, and z directions (Fig. 1(a)), respectively, where z was normal to the x-y plane of the solid surface. Initially, about 68 000 liquid atoms together with 160 nanoparticles were placed in a cubic lattice just above the solid surface. The liquid was initially relaxed at $T^* = 0.67$ to take the shape of a droplet surrounded by its vapor. Then a run of about 10 000 τ was performed at higher temperature ($T^* = 0.83$) to bring the solid, liquid, and vapor phases into thermal equilibrium. After equilibration, the droplet contained about 47 000 atoms on surface B with both three-phase contact lines located at the A-B boundaries (see Fig. 1(a)). The contact radius and contact angle after equilibration were about 20 nm and 67° , respectively. Note that because the droplet is pinned between the domains A and B, changing its volume would lead to contact angle values between 18° and 115° , which are the values on the pure B and A surfaces, respectively. In this case, the volume fraction of nanoparticles was about 4%. Periodic boundary conditions were used in the three dimensions of space. Due to the short extension of the system in the y direction (Fig. 1(a)), the equilibrium droplet had a cylindrical shape with its main axis oriented along the y direction. The main reason for choosing the cylindrical shape is to minimize the effect of the line tension, which was found to affect the evaporation mechanism of nanometer sized droplets.³² Additionally, cylindrical droplets make it possible to address systems with larger radii than spherical caps with the same number of particles.

All the simulations were carried out with LAMMPS.³⁰ The Berendsen thermostat³¹ with a coupling time 0.25τ was used to control temperature. The time-step and the cut-off distance were set to 0.0025τ (5 fs) and 4.4σ (1.5 nm), respectively. The evaporation was driven by deleting gas atoms from a deletion zone. The thermostat was used only for the solid atoms during the evaporation to mimic heating via the substrate. In our simulations, two different arrangements of the deletion zone were tested. In the first case, a rectangular box with a dimension of $171.5\sigma \times 18.9\sigma \times 29.4\sigma$ in the x, y, and

z directions was placed about 300σ above the solid. In the second case, a smaller rectangular box (dashed rectangle in Fig. 1(a)) was located immediately above surface A. This box has a height of 15σ in the z direction and a width with the same length as strip A in the y direction. In the x direction, this box boundary was placed at about 5σ away from the A-B boundary, i.e., from the TPCL area. We find that both setups generate very similar results at the same deletion rate. Therefore, we only show here the results from the second method.

To study the effect of the evaporation rate on the deposit pattern, we removed gas molecules at different rates from the simulation, namely, one molecule removed every 50, 200, 400, and 800 time steps (0.125, 0.5, 1, and 2τ , respectively). The simulations are denoted SX-50, SX-200, SX-400, and SX-800, respectively, where X denotes the system index (see Table I for details). For example, S1-50 means system S1 with a deletion rate of one gas molecule every 50 time steps. For each evaporation rate, four independent runs were performed to get better statistics.

To characterize the dynamics of evaporation, the temporal evolutions of droplet volume, density field, contact angle, and contact radius were computed. A cluster analysis method was applied to distinguish the liquid from vapor particles and to monitor the dynamics of the droplet volume. The spatial mass-density distribution was used to identify the liquid-vapor interface. As a result of the cylindrical geometry, this interface is represented by an isodensity contour line, which was used to calculate the contact angle values by following the same procedure as in our previous simulations.³² It should be mentioned that for a cylindrical droplet, the "contact radius" is defined as half the distance between the two contact lines.

III. RESULTS AND DISCUSSION

As mentioned above, we focus on the effect of two factors, namely, the liquid-nanoparticle interaction parameter ϵ and the evaporation rate on the shape of the deposit. We first discuss the influence of ϵ at the fastest evaporation rate, i.e., when deleting one gas atom every 50 time steps. Note that the nanoparticle-liquid interaction is stronger than the nanoparticle-nanoparticle interaction for all systems. Therefore, it is expected that the nanoparticles do not gather to form clusters, as is confirmed by the simulations discussed later in the text (Figs. 2(a), 3(a), 4(a), and 5(a)).

Fig. 2(a) shows the density of a droplet in equilibrium just before the evaporation is initiated. A higher density is visible at the liquid-vapor interface, suggesting that the nanoparticles initially accumulate at this boundary.

This is due to the fact that the interaction parameter for the liquid-nanoparticle interaction with a reduced value of $\epsilon^* = 0.8$ is obviously weaker than the parameter between liquid molecules ($\epsilon^* = 1.0$). In addition, the distance parameter for the nanoparticle-liquid interaction is equal to 1.1σ , which is larger than between the liquid particles (1.0σ). Therefore, the liquid-nanoparticle adhesive energy density is smaller than the cohesive energy density of the liquid but still larger than the characteristic energy density for the liquid-vapor interaction. As a result, the nanoparticles are forced to move to the interface during equilibration to decrease the liquid-vapor

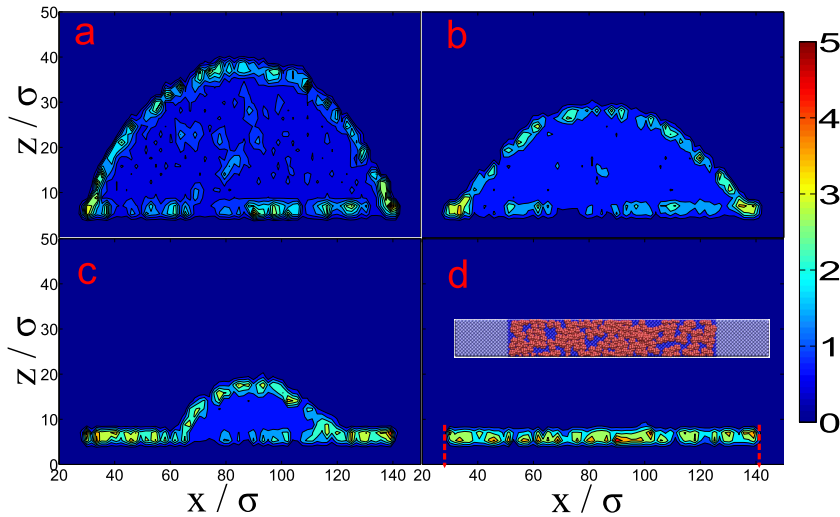


FIG. 2. Number density maps for the droplets of nanoparticle solution for system S1 at time $t =$ (a) 0τ , (b) $10\ 000\tau$, (c) $15\ 000\tau$, and (d) $30\ 000\tau$. The inset of (d) is a top view of the final deposition pattern as obtained from the last snapshot of the simulation trajectory. The vertical red dashed lines mark the position of the boundaries between the surfaces A and B. The density unit on the color bar is σ^{-3} .

interfacial energy of the system. This means that the nanoparticles replace interfacial liquid molecules and are in direct contact with vapor, although this would cause some entropy loss due to the confinement of the nanoparticles. Note that the nanoparticles at the interface do not form small clusters since their interaction with other nanoparticles is weaker than with the liquid. Therefore, they remain dispersed and can diffuse along the liquid-vapor interface.

After the evaporation is started by deleting gas molecules, the droplet's volume shrinks (black line in Fig. 3(a)), the contact angle decreases from its initial value of 67° (Fig. 3(b)). The contact lines are initially pinned at the A-B boundary with the corresponding pseudo-contact radius of about 58σ , i.e., about 20 nm (Fig. 3(c)). The number density of nanoparticles increases not only at the TPCL but also at the liquid-vapor interface as shown by the yellowish spots in Fig. 2(b). While liquid volume is further reduced, more nanoparticles gather at the interface and the liquid-vapor interface-enriched nanoparticles' layer becomes more visible. With further evaporation,

the contact angle keeps decreasing, while the contact radius starts to reduce when the evaporation time is larger than 5000τ . Once the contact lines recede, the vapor-interface-enriched nanoparticle layer begins to collapse onto the solid surface. When the evaporation time is above $10\ 000\tau$, the decrease in contact angle (Fig. 3(b)) slows down, while the decrease in contact radius (Fig. 3(c)) accelerates. The evaporation at this stage seems to follow the constant contact angle mode which is observed for cylindrical droplets of pure solvent on homogeneous surfaces.³² Note that the almost-constant receding contact angle is much larger than the equilibrium contact angle of the liquid on the pure surface B (18°). It is reasonable to assume that the adsorption of nanoparticles on the surface is responsible for this observation. Indeed, the nanoparticle-liquid interaction is less favorable than the surface-liquid interaction. It is thus expected that the wetting behavior of the surface with adsorbed particles is less favorable than the bare surface. Moreover, the adsorbed nanoparticles introduce roughness on the substrate. Roughness combined

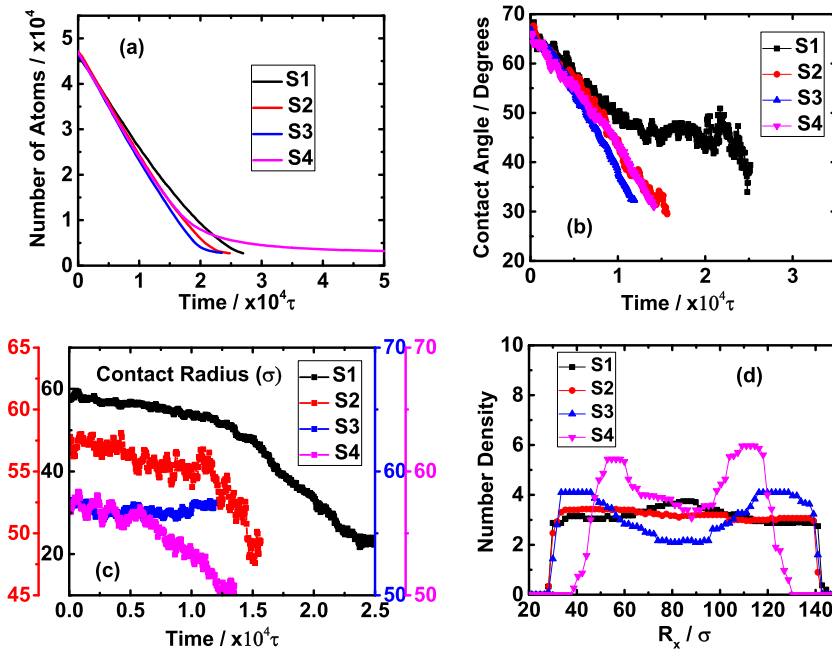


FIG. 3. All systems (S1–S4) with different liquid-nanoparticle interactions under the same deletion rate of one gas molecules per 50 time steps. (a) Time evolution of the number of atoms inside droplet. (b) Time evolution of the contact angles. (c) Time evolution of the contact radii. Note that all curves have their own y axes as indicated by the color to remove their overlap. (d) Nanoparticles' number density along x direction for the final deposits.

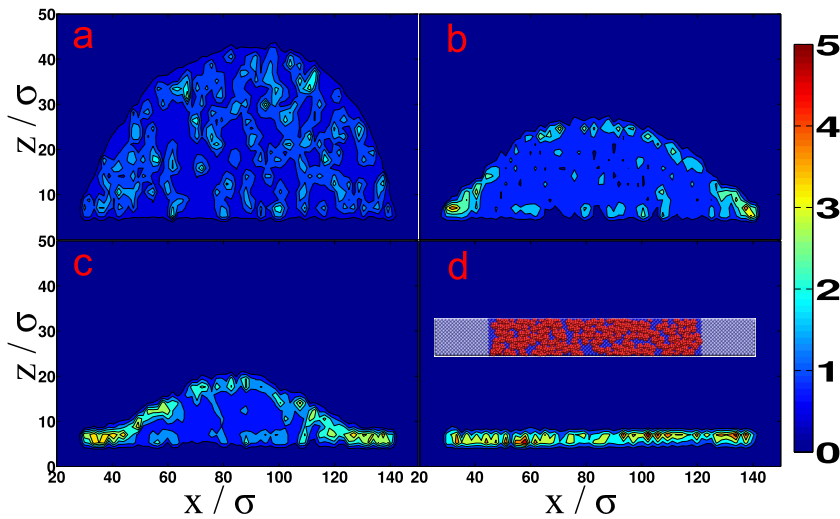


FIG. 4. Number density maps for the droplets of nanoparticle solution for system S2 at time $t =$ (a) 0τ , (b) $10\,000\tau$, (c) $15\,000\tau$, and (d) $30\,000\tau$. The inset in (d) is a top view of the final deposition pattern as obtained from the last snapshot of the simulation trajectory. The density unit on the color bar is σ^{-3} .

with the weak liquid-particle interaction increases the contact angle compared to the planar surface. During this period, the droplet keeps its spherical shape as illustrated in Fig. 2(c). Beyond $25\,000\tau$, the droplet experiences strong deformations due to its small size and the large density of the interfacial nanoparticle layer. When the liquid is completely evaporated, a deposit with a uniform density distribution is observed in the snapshot in Fig. 2(d). This uniform deposition pattern is confirmed by the number density distribution of nanoparticles along the x direction as shown by the black line in Fig. 3(d). Note that the black curve in Fig. 3(d) fluctuates around an average value of 3. These fluctuations mainly arise due to the limited size of the system. On the one hand, our simulation is 2D-like with the extent of the simulation domain in the y dimension relatively short. On the other hand, only one layer of nanoparticles is found in the final pattern. Moreover once the nanoparticles attach to the solid surface, they hardly move anymore. Due to these factors, obtaining a smoother curve simply by averaging over space and time is difficult. It is interesting to note that this result is very similar to the experiments³³ in which a uniform monolayer film of gold particles was observed when the particles were preferentially driven to the liquid-vapor interface by appropriate chemical modification of their surface.

When the liquid-nanoparticle interaction is increased to 0.9 in system S2, the solubility of the nanoparticles increases. The nanoparticles disperse rather homogeneously in the droplet (Fig. 4(a)) compared with system S1 (Fig. 2(a)).

When the droplet starts to evaporate, the contact angle decreases (Fig. 3(b)) while similarly to system S1 the pseudo contact radius fluctuates around its initial value of about 58σ (Fig. 3(c)). The nanoparticles show a clear trend of moving not only towards the contact lines but also towards the liquid-vapor interface during evaporation. This behavior is in contrast with system S1 in which the nanoparticles spontaneously migrated to the liquid-vapor interface due to their poor solubility. Consequently, an interfacial-enriched layer-like structure of nanoparticles builds up gradually (Fig. 4(b)). We calculated the number of nanoparticles that adsorb at the liquid-vapour interface for droplets with different volumes both under equilibrium and non-equilibrium conditions (see Fig. S1 and the related simulation details in the [supplementary material](#)). The results show that in the nonequilibrium situation (evaporation), more particles adsorbed at the interface than in equilibrium for the same droplet volume. It can be concluded that evaporation increases adsorption as compared to equilibrium. This situation arises from the fact that the liquid-vapor interface is receding faster than the nanoparticles can diffuse, as will be discussed below.

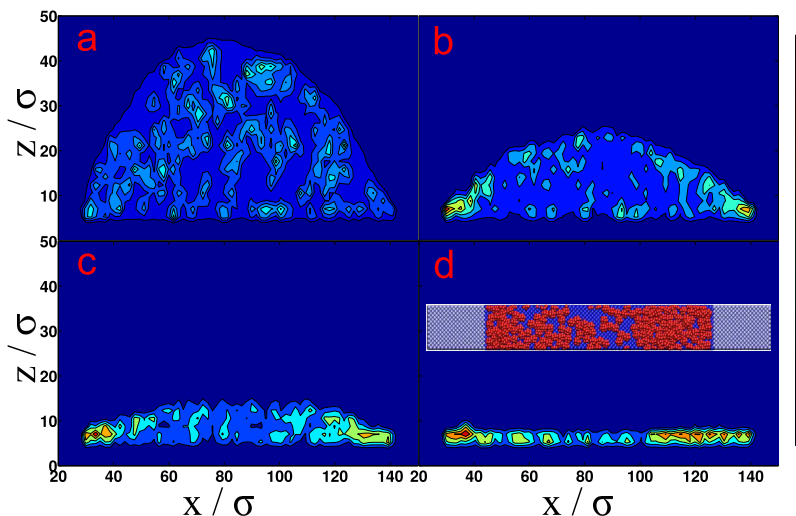


FIG. 5. Number density maps for the droplets of nanoparticle solution for system S3 at time $t =$ (a) 0τ , (b) $10\,000\tau$, (c) $15\,000\tau$, and (d) $30\,000\tau$. The inset in (d) is a top view of the final deposition pattern as obtained from the last snapshot of the simulation trajectory. The density unit on the color bar is σ^{-3} .

Besides, we observe that once the nanoparticles reach the liquid-vapor interface, some of them diffuse back into the bulk of the droplet. This phenomenon, which hardly occurs in system S1, might be caused by the nanoparticle's Brownian motion. Although the nanoparticle-liquid interaction in S2 is still weaker than the liquid-liquid interaction, the difference in S2 is reduced as compared to S1. Thus entropy drives mixing in S2, and nanoparticles are well dispersed (Fig. 4(a)). Different from S1, where the interactions keep the particles at the liquid-vapor interface, nanoparticles in S2 can diffuse back from the interfacial area to bulk. Furthermore, it can be observed that the density of the interface-enriched nanoparticle layer (Fig. 4(b)) is not as large as in system S1 (Fig. 2(b)).

With further evaporation, more nanoparticles gather at the liquid-vapor interface. Meanwhile, the contact angle (Fig. 3(b)) keeps decreasing while the pseudo contact radius (Fig. 3(c)) remains constant (pinned contact lines) until approximately $10\,000\tau$. After that, the pseudo contact radius (Fig. 3(c)) starts to decrease, the droplet then reduces its volume with moving contact lines. At the same time, the vapor-interfacial nanoparticle layer starts to collapse onto the solid surface. Fig. 4(c) shows the overall shape of the droplet at time $t = 15\,000\tau$, the droplet already deforms due to the deposited nanoparticles at the edges. Calculating the contact angle and the contact radius for the deformed droplet is a difficult task. At a late stage of evaporation, the droplet's volume shrinks quickly. The whole nanoparticle-enriched interfacial layer eventually collapses onto the solid surface and generates a uniform deposit (Fig. 4(d)). This observation is quantified by the number density distribution of nanoparticles in the deposit along the x direction shown by the red line in Fig. 3(d). From the simulations of S1 and S2, one might come to the conclusion that the vapor-interface-enriched layer of nanoparticles, no matter whether it is interaction-driven or evaporation-induced, would lead to form a uniform pattern after the droplet completely evaporates.

A similar phenomenon¹⁹ of evaporation-driven nanoparticle layer has been reported very recently by Li *et al.* In experiments about the evaporation of water droplets (diameter > 1 mm) with spheres of hydrophilic polystyrene, these authors found that fast evaporation generated a uniform rather than ring-like pattern. They explained this phenomenon by the competition between the rate at which the interface shrinks and the diffusion rate of the nanoparticles. For fast-enough evaporation, the interface collapses relatively faster than the transport of nanoparticles through diffusion, the nanoparticles near the interface are thus trapped at the fast-moving interface. As a result, an evaporation-induced interfacial layer of particles is formed during evaporation. At the end of the evaporation, the interfacial layer of nanoparticles transforms into a uniform deposit. In order to compare qualitatively our nanoscale results with macroscopic experiments, we calculated the Péclet number Pe following $Pe = (\text{interface receding rate})/(\text{diffusion rate})$. The interface receding rate was calculated as the velocity with which the top of the droplet descended. The approximate value $2.1 \times 10^{-3}\sigma/\tau$ was obtained. The diffusion rate of the nanoparticles in the liquid argon droplet was calculated as the ratio between the self-diffusion coefficient D^* of the nanoparticles and their diameter $d^* \approx 6$. We found $D^* \approx 7.0 \times 10^{-3}\sigma^2/\tau$ (D

$\approx 4.1 \times 10^{-10}$ m²/s), which yields $Pe \approx 2$ for system S2. This value indicates that the liquid-vapour interface recedes faster than that the nanoparticles in the vicinity of the interface can diffuse. It is interesting to note that that value of Pe is comparable with what was observed in Fig. 4(c) of the work of Li *et al.*¹⁹ at about 55 °C where almost uniform deposits were obtained. Our simulations on the one hand confirm the results of Li *et al.* and on the other hand highlight the important role played by the nanoparticles' solubility in determining the final pattern. A certain parameter range (i.e., a certain kind of wetting properties of the nanoparticles) might be needed to observe the evaporation-induced nanoparticle layer phenomenon. In fact, we will show later that with the same size of nanoparticle and the same removal rate of gas molecules, the evaporation-induced layer only clearly appears in this S2 system.

For system S3, the same interaction strength between the liquid particles and between liquid and nanoparticles is used. The density evolution is plotted in Figs. 5(a)–5(d). Similarly to S2, the nanoparticles are initially dispersed inside the droplet as described in Fig. 5(a).

Once the evaporation is triggered, the contact angle (blue line in Fig. 3(b)) starts to decrease while the contact lines (blue line in Fig. 3(c)) are pinned, similarly to S1 and S2. In contrast to S1 and S2, the nanoparticles gather next to the contact lines, rather than at the liquid-vapor interface, during the evaporation (Fig. 5(b)). With further evaporation, the contact angle keeps decreasing and the contact line remains pinned. The number of nanoparticles that are deposited in the contact line region constantly increases. Owing to the favorable nanoparticle-liquid interaction, the deposited nanoparticles are wetted by the liquid better than the substrate surface, strengthening the pinning of the liquid contact lines. Consequently, the droplet gradually becomes flatter (Fig. 5(c)) with a pinned contact radius (blue line in Fig. 3(c)). In this case, the droplet is more like a thin film. We also observe that the contact lines remain pinned until the end of the evaporation.

In the end, a relatively high number density area around the contact lines is found after the droplet completely evaporated as shown in Fig. 5(d), indicating a non-uniform deposit pattern with more particles at edge than in the middle, i.e., an approximate "ring-like" structure in three dimensions. The final snapshot of the deposit (inset in Fig. 5(d)) clearly shows its non-uniform structure. The density distribution of nanoparticles along the x direction (blue line in Fig. 3(d)) confirms that the final pattern contains more particles at the edges than in the middle. This coffee-ring pattern is very often reported in experiments.^{1,19} It is caused by the pinned contact lines and faster evaporation at the droplet edge. Note that the density contrast between the middle region and the edges in Fig. 3(d) is not as large as in experiments. One possible reason is that the droplet used here has nanometer sized dimensions (initial contact radius of about 20 nm) and is much smaller than in experiments. Smaller droplets possess smaller edge areas, and multilayer deposits of nanoparticles are therefore harder to form. Using smaller droplets also means that evaporation completes in shorter times, it is therefore difficult to form a strong outward flow to drive the nanoparticles towards the edges. One may wonder whether a faster evaporation can generate a

deposit with a clearer ring-like structure in the S3 system. Our simulations suggest that this will probably not be the case, as is discussed below together with the effect of the evaporation rate in S3. In addition, two recent molecular dynamics simulations of salty-water droplets²⁴ and liquid droplets with nanoparticles²³ also showed ring-like deposits. However, it should be noted that, in both these simulations, the droplets were spreading when the evaporation took place. This process was caused either by the increase of the substrate's temperature²⁴ or by the strong liquid-substrate interaction.²³ It is not clear what effect the spreading behavior of the droplet has on the final pattern. Furthermore, Chen *et al.*²³ stated that in contrast to our results, the liquid-particle interaction has very little effect on the shape of the final pattern.

For system S4, the liquid-nanoparticle interaction is stronger than the liquid-liquid one. The density maps are shown in Figs. 6(a)–6(d). Similarly to S2 and S3, the nanoparticles in S4 are initially dispersed in the droplet (Fig. 6(a)). Interestingly, not only the contact angle (Fig. 3(b)) but also the pseudo contact radius (Fig. 3(c)) decreases from the beginning of the evaporation. This behavior differs from the other three systems discussed above, where the pseudo contact radius remains constant at least during the early stage of the evaporation. The receding motion of the contact lines presumably arise from the strong interaction between the contact line and the nanoparticles. In fact, in system S4, the nanoparticle-liquid interaction ($\epsilon^* = 1.6$) is much stronger than the liquid-liquid ($\epsilon^* = 1.0$) and nanoparticle-surface-B ($\epsilon^* = 0.9$) interactions. Thus, the nanoparticles cannot stick to the solid surface near the TPCL and the moving nanoparticles near the TPCL drag the contact line towards the center of the droplet. Therefore, the contact line is receding instead of being pinned at the surface A-B boundary during evaporation.

As evaporation continues, the density of the nanoparticles increases with time, but the density distribution is not uniform as can be seen in Fig. 6(b). The nanoparticles appear less in the center than in any other area of droplet. This non-uniform concentration of nanoparticles should arise from the fast inward motion of the contact lines and the vapor interface, with which the slowly diffusing nanoparticles cannot keep up. When the droplet volume further reduces, both the contact angle and the

pseudo contact radius continue decreasing, while the droplet shape gradually changes from spherical to thin-film-like. The vapor interface is curved near the TPCL, but almost flat at the droplet centre (Fig. 6(c)).

In the end, when the thin-film-like droplet disappears completely, the deposit has a volcano shape (Fig. 6(d)). The width of the final deposit is obviously narrower for S4 than for the other three systems (Fig. 3(d)). Such shapes have also been reported for polymer solution systems.^{34,35} For instance, Kajiya³⁴ reported that the receding contact line left a volcano-like pattern after drying a droplet of a water-poly(N,N-dimethylacrylamide) solution. Such a receding contact line also plays a key role for our simulated volcano-like pattern.

These results clearly show that the solubility of the nanoparticles in the liquid indeed dominates the final shape of the deposits. In experiments, the interaction strength of the nanoparticle-liquid can be varied by surface coating or grafting. Our simulations show that the nanoparticle-liquid interaction also influences the evaporation dynamics. Although evaporation is driven by the removal of gas molecules at the same rate in the four simulated systems, the droplet volumes decrease at different speeds. As shown in Fig. 3(a), S1 is the slowest due to the dense layer of interfacial-nanoparticles, while S3 was the fastest, with the other two falling in between. Note the strong slowdown for the evaporation in S4 (magenta curve in Fig. 3(a)) at the late stage, due to the strong interactions between the last liquid atoms and the already precipitated nanoparticles.

We now turn to the role of the evaporation rate. First, it is clear that slower evaporation would not change the final uniform pattern of S1, since the uniform shape of the deposit arises from the enrichment of the nanoparticles at the liquid-vapor interface due to their low solubility. Reducing the evaporation rate does not change this mechanism and would thus not change the shape of the pattern. Therefore, we present here only the results for the three other systems, namely, S2, S3, and S4.

As discussed above about Fig. 4 for system S2, evaporation-induced nanoparticle enrichment at the liquid-vapor interface appears at the fast removal rate of one gas molecule every 50 time steps. We also study three slower

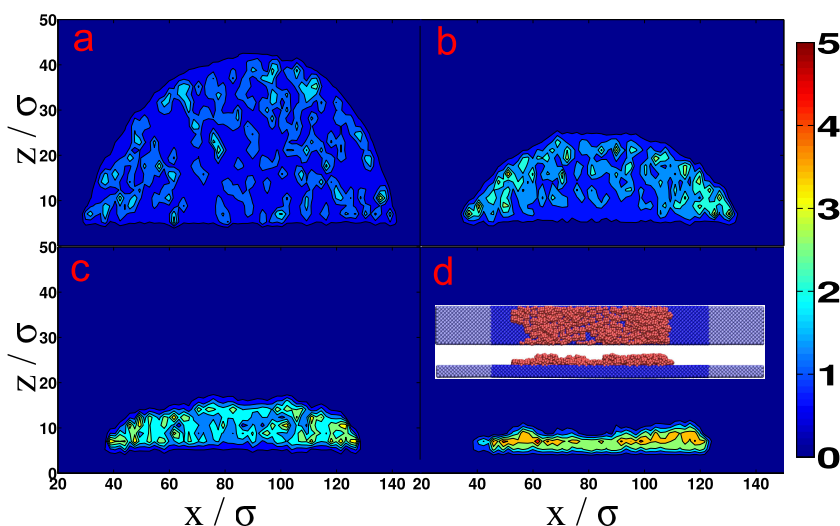


FIG. 6. Number density maps for the droplets of nanoparticle solution for system S4 at time $t =$ (a) 0τ , (b) $10\,000\tau$, (c) $15\,000\tau$, and (d) $50\,000\tau$. The inset in (d) represent a top view (upper panel) and side view (lower panel) of the final deposition pattern as obtained from the last snapshot of the simulation trajectory. The density unit on color bar is σ^{-3} .

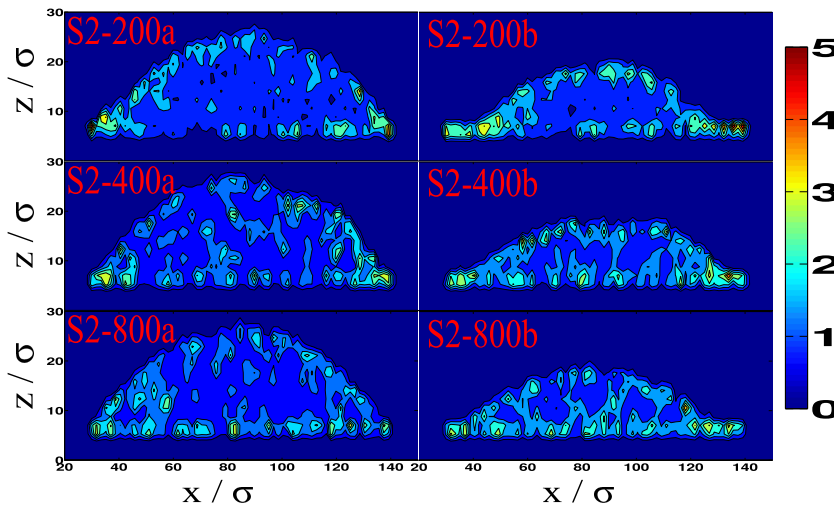


FIG. 7. Number density maps for the droplets of nanoparticle solution for system S2 at three evaporation rates induced by three different removal rates of deleting one gas molecule at every 200, 400, and 800 time steps. The labels a and b refer to droplet sizes containing about 24 400 and 14 100 atoms, respectively. The density unit on color bar is σ^{-3} .

evaporation rates for this system. To quantitatively compare the results with the fastest evaporation rate shown in Fig. 4, we plot two density maps for each deletion rate in Fig. 7. The two maps correspond to two droplets at the times where they contain approximately 24 400 (plot S2-200a, S2-400a, and S2-800a) and 14 100 particles (S2-200b, S2-400b, and S2-800b). The labels a and b refer to droplet sizes, in contrast to the above density plots where they referred to evaporation times. In both a and b plots, the shape of the droplet is very close to what can be seen in Fig. 4(b) and in Fig. 4(c), respectively.

With lower deletion rate, the droplet volume decreases more slowly (Fig. 8(a)). Note that, for all evaporation rates, the volume decreases linearly with time, except for the late stage of evaporation. This result is in line with the prediction of Popov's model for the time dependence of the droplet mass.³⁶ When comparing the number density profiles of S2-200a, S2-400a, and S2-800a in Fig. 7 together with Fig. 4(b), we observe that the structure of the interfacial layer of nanoparticles becomes

more diffuse with decreasing evaporation rate. Consequently, the density contrast between the liquid-vapor interface and the bulk decreases. A similar trend is found for the second droplet size, as can be seen from Fig. 7 (S2-200b, S2-400b, and S2-800b). Therefore, we confirm that a fast evaporation rate can indeed induce a layer-like structure of nanoparticles at the liquid-vapor interface in system S2.

The final deposition patterns may also be affected by the slower evaporation rates (Figs. 8(b)–8(d)). For S2 (Fig. 8(b)), all final density distributions are uniform, although with fluctuations. Therefore, evaporation rate does not show a notable effect on the final deposit structure of system S2.

Recall that system S3 (Fig. 5(d)) forms a ring-like deposit for fast evaporation. Therefore, it may be expected that the evaporation rate plays a role on the deposition pattern. We found that the ring-like pattern gradually disappears for the smaller deletion rates. This is also evident in the final nanoparticles' deposits (Fig. 9) and density profiles (Fig. 8(c)).

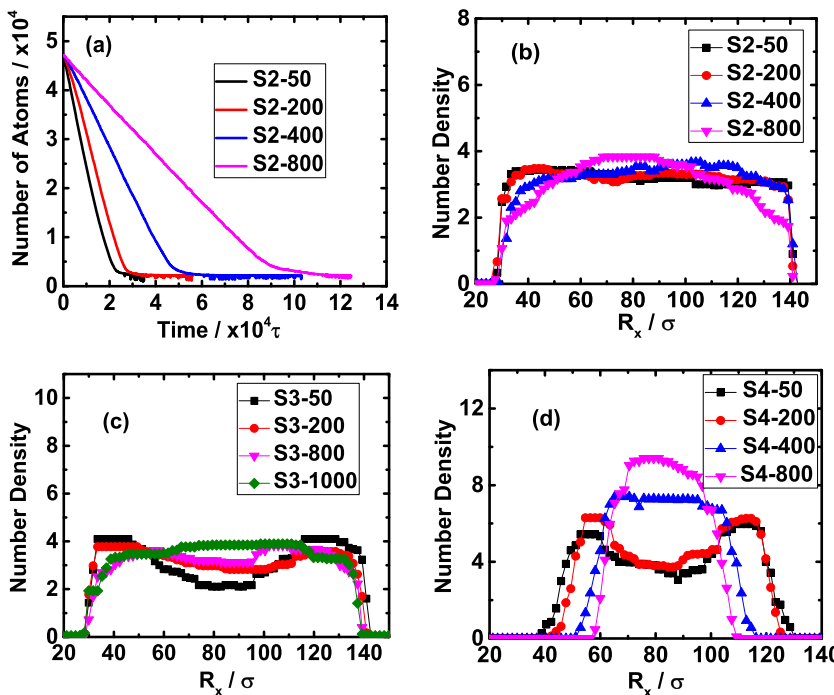
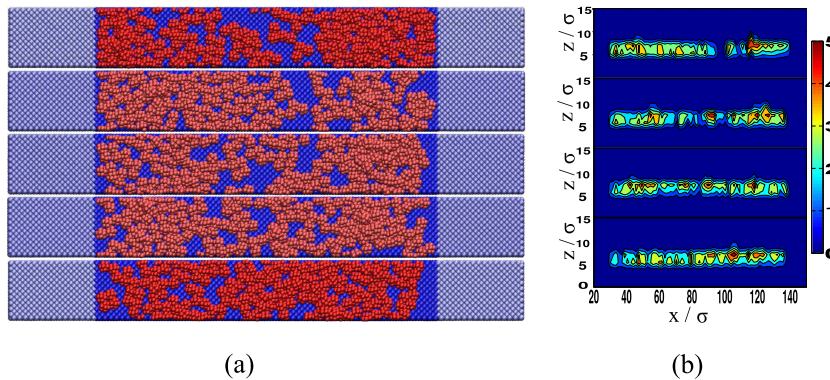


FIG. 8. (a) Time evolution of number of atoms inside droplet for system S2 at different evaporation rates. Number density distribution of nanoparticles along x direction for systems (b) S2, (c) S3, and (d) S4 at different evaporation rates. SX-200, SX-400, SX-800, and SX-1000 indicate a removal rate of one gas molecule per 50, 200, 400, 800, and 1000 time steps, respectively. X is the system label.



(a)

(b)

All representations confirm that an increasing number of nanoparticles are deposited on the central part of the final pattern with slower evaporation rates. Thus the density in the middle part becomes comparable to that at the edges. Thus, the evaporation rate indeed matters for the system S3. A fast rate induces ring-like patterns while a slower one generates a more uniform structure. The possible reason is that the nanoparticles will have enough time to diffuse back from the TPCL region to the bulk with slower evaporation rate. As a proof, the calculated diffusion coefficient of nanoparticles in the liquid is $D^* \approx 5.5 \times 10^{-3} \sigma^2/\tau$ ($3.2 \times 10^{-10} \text{ m}^2/\text{s}$). They can diffuse a distance of about 140σ (47 nm) along one direction within the lifetime ($1.5 \times 10^5 \tau$) of the droplet in S3 when deleting one gas molecule every 1000 time steps. This distance is more than two times the droplet height and the calculated Peclet number is $P_e \approx 0.4$.

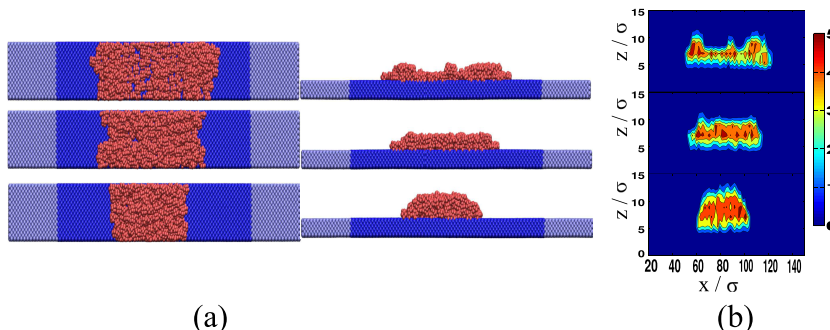
The final pattern in Fig. 5(d) for system S3 is not “perfectly” coffee-ring-like in the sense that it does not exhibit a wide empty space between narrow deposits of the nanoparticles at the droplets edges. Therefore, we performed a simulation at an even faster deletion rate of one gas molecule every 20 time steps with the intent to enhance the effect obtained at the rate of one molecule every 50 steps. Unfortunately, the obtained result does not show such an enhancement in the final structure as illustrated by a snapshot of the final pattern in Fig. S2(a) in the [supplementary material](#). The possible reason is that, at this removal rate, the diffusion in the gas phase becomes the bottleneck for evaporation. It was found that the mean-free path of the gas molecules is at least one order of magnitude lower than the dimensions of the system. Thus the Knudsen number is significantly smaller than 1, indicating the importance of diffusion in the gas phase. In fact the deletion rate of gas molecules in the deletion zone does not

necessarily increase the evaporation rate if the deletion rate is already frequent enough and if there is no gas left in the deletion zone. A deletion rate of one gas molecule every 50 time steps in our simulations seems to be close to the reachable limit.

Fig. 10 shows the final deposits of the very soluble system S4 at three different evaporation rates. Their high solubility keeps the nanoparticles in solution. This prevents their early deposition onto the substrate, and thus, they are transported with the receding contact line.

The side views of the final deposition pattern snapshots in Fig. 10(a) show that the width of the final stain along the x direction decreases with decreasing the evaporation rate, which is consistent with this picture. The pattern changes from volcano-like at a removal rate of 200 to pancake-like at a removal rate of 800. The density maps (Fig. 10(b)) and the nanoparticle number density distribution along the x direction (Fig. 8(d)) confirm these results. Therefore, the evaporation rate has an important effect on the final pattern in system S4. Our results are in line with the recent theoretical work of Man and Doi²⁰ who proposed a theoretical model with two adjustable parameters to control the motion of the contact line and the evaporation rate. They predicted deposition patterns whose shape changed from ring-like to volcano-like and further to mountain-like by increasing the speed of the contact line and lowering the evaporation rate. Besides, our results indicate that the strong liquid-nanoparticle interaction is the reason for the contact line to unpin and to recede during evaporation for system S4 while they stay pinned for the other systems with weaker liquid-nanoparticle interaction.

For completeness, a simulation with one gas molecule deleted every 20 time steps was performed. The resulting pattern has a volcano-like shape which is only slightly more



(a)

(b)

FIG. 10. S4 at three different evaporation rates. (a) Snapshots of final patterns. Left panels were the top view, while the right panels were side view. (b) Density maps of final deposit patterns. In both profiles, panels from top to bottom referred to simulations with deleting one gas atom at every 200, 400, and 800 time steps, respectively.

pronounced compared with the slower removal rate of 1 molecule every 50 steps as illustrated by a snapshot in Fig. S2(b) in the [supplementary material](#).

IV. CONCLUSION

The formation of deposits of nanoparticles and their structure after the drying of nanosized droplets of nanoparticle suspensions on solid surfaces was studied by molecular dynamics simulations. The surface was made energetically heterogeneous to pin the contact lines. The influence of two factors on the shape of the final deposition patterns was investigated especially, namely, the nanoparticle-liquid interaction strength (i.e., their solubility) and the evaporation rate. The nanoparticle-liquid interaction can experimentally be tuned by chemical surface treatments or grafting with polymer chains. In our simulations, its effect was investigated in a systematic way through a single energy parameter whose magnitude was adjusted in a range such that the particles were switched from insoluble to well soluble. We find that both factors play an important role for the evaporation process and the pattern of the final deposit. Our results provide a molecular level explanation of the mechanism of the pattern formation of coffee stain observed in some experiments and more importantly highlight the importance of the compatibility of the nanoparticles with the solvent, which has not been emphasized so far. The main results are summarized below as follows:

- (a) The nanoparticles accumulated at the liquid-vapor interface and formed there an interfacial layer when they were insoluble (system S1). This structure was observed both in the equilibrium state before evaporation and out of equilibrium during evaporation. The contact lines were pinned at the early stage of evaporation and then receded towards the center of the droplet at the late stage of evaporation. When the contact lines receded, the nanoparticle layer at the vapor interface was gradually driven towards the solid surface and eventually formed a structure with a uniform distribution of particles when the solvent completely disappeared. When the nanoparticle-solvent interaction strength was increased, the nanoparticles were dispersed throughout the droplet at equilibrium. When evaporation was started, the contact lines showed a behavior similar to what is described above for the insoluble system S1, i.e., they were pinned during a certain period of time before they finally receded. The formation of an enrichment layer of nanoparticles at the vapor-interface was not observed in equilibrium, but only during evaporation. We thus conclude that the formation of this layer is an evaporation-induced non-equilibrium transient, caused by the shrinking of the droplet being too fast for the nanoparticles to redisperse by diffusion. This is in contrast to system S1 whose particles were already insoluble at equilibrium. Similar to system S1, however, this nanoparticle layer gradually migrated towards the solid surface onto which it finally collapsed into a rather uniform deposit. We further increased nanoparticle-solvent interaction to a value equal to the solvent-solvent interaction (system

S3). In this case, the contact line remained pinned during the whole evaporation process, as the remaining solvent could now wet the already deposited nanoparticles. This led to a non-uniform deposit with more nanoparticles at the edges than at the middle. This could be construed as the emergence of a coffee-ring-like pattern. A further increase of the nanoparticle-solvent interaction (system S4) caused unpinning of the contact line all the way through evaporation. The receding contact line carried most of the nanoparticle with it, concentrating them. The final deposit had the shape of a volcano in this case.

- (b) Also the evaporation rate influences the evaporation process and the final structure of the deposit. In system S2, the dynamic, evaporation-induced enrichment of nanoparticles near the vapor interface was weaker for slower evaporation: Slower inward motion of this interface gives the nanoparticles time to redistribute throughout the droplet by diffusion. Correspondingly, for this weakly soluble system, the evaporation rate had a weak effect on the shape of the final pattern. In system S3, where the solvent-solvent and nanoparticle-solvent interactions are balanced, this redistribution was even stronger, such that the coffee-ring pattern found at fast solvent evaporation disappears, when evaporation is slower. As a consequence, a more uniform deposit is left behind. Finally, well-soluble nanoparticles avoid the droplet interfaces altogether. They are concentrated by the shrinking droplet. At fast evaporation, the precipitate in a volcano-like shape with higher rims and a lower, but still thick, inner part. If a low evaporation rate gives them more time to avoid local supersaturation they form into a film of uniform thickness, and at the lowest rates into a mountain shape. All observations are in line with the concept of a competition between the receding motion of the contact lines and the diffusion of the nanoparticles.

All the final deposition patterns shown here are case-based and depend on the parameters setting, they might be susceptible to other parameters like nanoparticle concentration. Nevertheless, our studies indicate that it may be possible to control the desired structure of a deposit, like a homogeneous sample for MALDI mass spectrometry,³⁷ or like a thin film or nanowires of certain width and thickness for nanotechnology,¹³ not only by a system parameter like the solubility or the chemistry of the nanoparticle surface but also by a process parameter like the solvent evaporation rate.

SUPPLEMENTARY MATERIAL

See the [supplementary material](#) for adsorption of nanoparticles at liquid-vapor interface for droplets with different volumes and under both nonequilibrium and equilibrium conditions, and for the snapshots of the final deposits for systems S3 and S4 with deleting one gas atom at every 20 time steps.

ACKNOWLEDGMENTS

We would like to thank for the financial support by the Collaborative Research Centre Transregio 75 Droplet Dynamics

in Extreme Environments of the Deutsche Forschungsgemeinschaft. The authors thank an anonymous reviewer for very constructive comments.

- ¹R. D. Deegan, O. Bakajin, T. F. Dupont, G. Huber, S. R. Nagel, and T. A. Witten, *Nature* **389**, 827 (1997).
- ²S. Khapli, I. Rianasari, T. Blanton, J. Weston, R. Gilardetti, R. Neiva, N. Tovar, P. G. Coelho, and R. Jagannathan, *ACS Appl. Mater. Interfaces* **6**, 20643 (2014).
- ³D. Xia and S. Brueck, *Nano Lett.* **4**, 1295 (2004).
- ⁴M. Kuang, L. Wang, and Y. Song, *Adv. Mater.* **26**, 6950 (2014).
- ⁵R. D. Deegan, O. Bakajin, T. F. Dupont, G. Huber, S. R. Nagel, and T. A. Witten, *Phys. Rev. E* **62**, 756 (2000).
- ⁶H. Hu and R. G. Larson, *J. Phys. Chem. B* **110**, 7090 (2006).
- ⁷Y. Li, C. Lv, Z. Li, D. Quéré, and Q. Zheng, *Soft Matter* **11**, 4669 (2015).
- ⁸M. Parsa, S. Harmand, K. Sefiane, M. Bigerelle, and R. Deltombe, *Langmuir* **31**, 3354 (2015).
- ⁹T. Still, P. J. Yunker, and A. G. Yodh, *Langmuir* **28**, 4984 (2012).
- ¹⁰H. B. Eral, D. M. Augustine, M. H. Duits, and F. Mugele, *Soft Matter* **7**, 4954 (2011).
- ¹¹H. B. Eral, D. van den Ende, and F. Mugele, *Phys. World* **25**, 33 (2012).
- ¹²X. Zhong, A. Crivoi, and F. Duan, *Adv. Colloid Interface Sci.* **217**, 13 (2015).
- ¹³J. Sun, B. Bao, M. He, H. Zhou, and Y. Song, *ACS Appl. Mater. Interfaces* **7**, 28086 (2015).
- ¹⁴C. H. Chon, S. Paik, J. B. Tipton, and K. D. Kihm, *Langmuir* **23**, 2953 (2007).
- ¹⁵T.-S. Wong, T.-H. Chen, X. Shen, and C.-M. Ho, *Anal. Chem.* **83**, 1871 (2011).
- ¹⁶P. J. Yunker, T. Still, M. A. Lohr, and A. Yodh, *Nature* **476**, 308 (2011).
- ¹⁷D. Brutin, *Colloids Surf., A* **429**, 112 (2013).
- ¹⁸D. Mampallil, J. Reboud, R. Wilson, D. Wylie, D. R. Klug, and J. M. Cooper, *Soft Matter* **11**, 7207 (2015).
- ¹⁹Y. Li, Q. Yang, M. Li, and Y. Song, *Sci. Rep.* **6**, 24628 (2016).
- ²⁰X. Man and M. Doi, *Phys. Rev. Lett.* **116**, 066101 (2016).
- ²¹L. Frastia, A. J. Archer, and U. Thiele, *Phys. Rev. Lett.* **106**, 077801 (2011).
- ²²N. Lebovka, S. Khrapatiy, R. Melnyk, and M. Vygornitskii, *Phys. Rev. E* **89**, 052307 (2014).
- ²³W. Chen, J. Koplik, and I. Kretzschmar, *Phys. Rev. E* **87**, 052404 (2013).
- ²⁴J. Zhang, M. K. Borg, K. Sefiane, and J. M. Reese, *Phys. Rev. E* **92**, 052403 (2015).
- ²⁵J. Zhang, M. K. Borg, K. Ritos, and J. M. Reese, *Langmuir* **32**, 1542 (2016).
- ²⁶A. Crivoi, X. Zhong, and F. Duan, *Phys. Rev. E* **92**, 032302 (2015).
- ²⁷A. Crivoi and F. Duan, *Langmuir* **29**, 12067 (2013).
- ²⁸W. Humphrey, A. Dalke, and K. Schulten, *J. Mol. Graphics* **14**, 33 (1996).
- ²⁹J. Zhang, F. Müller-Plathe, and F. Leroy, *Langmuir* **31**, 7544 (2015).
- ³⁰S. Plimpton, *J. Comput. Phys.* **117**, 1 (1995).
- ³¹H. J. Berendsen, J. P. M. Postma, W. F. van Gunsteren, A. DiNola, and J. Haak, *J. Chem. Phys.* **81**, 3684 (1984).
- ³²J. Zhang, F. Leroy, and F. Müller-Plathe, *Phys. Rev. Lett.* **113**, 046101 (2014).
- ³³T. P. Bigioni, X.-M. Lin, T. T. Nguyen, E. I. Corwin, T. A. Witten, and H. M. Jaeger, *Nat. Mater.* **5**, 265 (2006).
- ³⁴T. Kajiyama, C. Monteux, T. Narita, F. Lequeux, and M. Doi, *Langmuir* **25**, 6934 (2009).
- ³⁵K. Fukuda, T. Sekine, D. Kumaki, and S. Tokito, *ACS Appl. Mater. Interfaces* **5**, 3916 (2013).
- ³⁶Y. Popov, *Phys. Rev. E* **71**, 036313 (2005).
- ³⁷J. B. Hu, Y. C. Chen, and P. L. Urban, *Anal. Chim. Acta* **766**, 77 (2013).